Microengineered three-dimensional collagen fiber landscapes with independently tunable anisotropy and directionality

Adeel Ahmed[1], Indranil M. Joshi[2], Stephen Larson[2], Shayan Gholizadeh[1,2], Farzad Forouzandeh[1,3], David A. Borkholder[1,3], Thomas R. Gaborski[1,2], and Vinay V. Abhyankar[1,2,*]

[1]Department of Microsystems Engineering, [2]Department of Biomedical Engineering, [3]Department of Electrical Engineering

Rochester Institute of Technology, Rochester, NY, 14623, USA

*e-mail: vvabme@rit.edu

Keywords: Collagen I, microengineering, anisotropy, interfaces, tissue engineering

Abstract

Fibrillar collagen is abundant in the extracellular matrix (ECM), and cellular processes including differentiation, proliferation, and migration, have been linked to the directionality and degree of alignment (anisotropy) of collagen fibers. Given the importance of cell-substrate interactions in driving biological functions, several microfluidic approaches have been developed to create three-dimensional (3D) collagen gels with defined fiber properties that enable quantitative correlations between structural cues and observed cell responses. Although existing microfluidic methods provide excellent control over collagen fiber anisotropy, independent control over both fiber direction and anisotropy (that we collectively refer to as the "collagen landscape") has not been demonstrated. Therefore, to advance collagen microengineering capabilities, we present a user-friendly approach that uses fluid flows to create well-defined collagen landscapes within a microfluidic channel network. These landscapes include: i) control over fiber anisotropy, ii) spatial gradients in fiber anisotropy, and iii) defined fiber directionality. Finally, we present two approaches to simplify procedures to allow cell interaction with the microengineered collagen landscapes.

Introduction

The extracellular matrix (ECM) is the non-cellular component of native tissue and is composed primarily of glycosaminoglycans (GAGs), proteoglycans, and fibrillar proteins such as type I, II, III, and V collagen[1]. Besides providing structural support, the fibrous ECM proteins play an essential role in regulating cell behavior in both physiological and pathophysiological processes. For example, reciprocal interactions between cells and ECM result in the dynamic remodeling of the local environment to create domains with defined type I collagen fiber alignment (*i.e.,* anisotropy) and directionality[2,3]. The resulting collagen landscapes have been shown to modulate the motility of T-cells[4], guide endothelial cell alignment[5], support stem cell "stemness"[6], regulate cell differentiation[7], and enhance wound healing[8]. Fiber landscapes have also been found to be a prognostic indicator of breast cancer patient survival[9,10]l. Given the importance of the collagen microarchitecture in a variety of biological processes, there have been significant efforts to create *in vitro* platforms that can replicate physiological fiber landscapes to study cellular responses in a controlled manner.

Several methods including the use of magnetic beads[11,12], application of mechanical strain[13,14], cell-based compaction[15,16], electrospinning[17,18], and 3D printing approaches[19,20] have been used to create anisotropic collagen fibers *in vitro*. Even though current methods provide control over collagen fiber anisotropy, they are unable to combine these fiber domains with cellular scale control over physiologically relevant biophysical and biochemical cues that are possible using microfluidic approaches[21,22]. Although the current class of microfluidic systems can achieve high levels of fiber anisotropy using fluid flows or the application of mechanical forces[23–25], they are unable to achieve the independent control over fiber anisotropy and directionality needed to

replicate the diverse structural environments found *in vivo*[12,23,24]. In addition, conventional microfluidic systems are sealed, and the introduction of cells is achieved by i) embedded them in the gel solution during the device filling process, or ii) using pre-defined side channels or ancillary access ports. These requirements limit both the experimental flexibility and ease of use for microfluidic approaches.

The goals of this work are two-fold: first, we introduce a microfluidic approach that uses mixed shear and extensional flows of type I collagen solutions within a variable cross-sectional area microfluidic network to create well-defined anisotropic collagen fiber domains, spatial gradients in fiber anisotropy, and control over fiber directionality. Second, we address the practical challenge of introducing cells to our collagen landscapes by demonstrating i) a process to remove the microfluidic channel network after gel formation and ii) the inclusion of a sub-micron thin membrane with defined pores as the "ceiling" of the microfluidic channel network.

Experimental

PDMS Device Fabrication

Microfluidic channels were fabricated using standard soft photolithography techniques. Briefly, SU-8 3050 (Kayaku Advanced Materials, Massachusetts, USA)) was spin-coated to a thickness of 0.06 mm on a silicon wafer (University Wafers, South Boston, USA), soft-baked, exposed to UV light through a photomask, and developed. A 10:1 prepolymer base to crosslinker ratio (Sylgard 184, Dow Corning, Midland, USA) was poured over the master mold and cured for 2 hours at 80˚C on a hotplate to form the final channels. Inlet ports were punched using a 1mm biopsy punch. Channel dimensions are shown in **Figure S1.**

Surface functionalization

PDMS channels were functionalized by immersion in a 10 mg ml^{-1} bovine serum albumin solution in PBS (Fisher Scientific, Pittsburgh, USA) for 4 hours at 2˚C. Glass coverslips were coated with poly(octadecene-alt-maleic anhydride) using the method described by Pompe et al. [26]. Briefly, coverslips were sonicated for 5 minutes in 70% ethanol and dried under an airstream. The coverslips were then exposed to O_2 plasma for 60 s under 600mTorr at high setting (Harrick Plasma, Ithaca, NY, USA), and then submerged in a solution containing 2% aminopropyltriethoxysilane (APTES) (Millipore Sigma, Burlington, USA), 90% ethanol, 5% deionized water, and 3% glacial acetic acid. The coverslips were lightly agitated (5 minutes) and placed on a hot plate at 110˚C for 10 minutes. Next, a 0.8 mg/mL solution of poly(octadecene maleic alt-1-anhydride) (Millipore Sigma, Burlington, USA) dissolved in tetrahydrofuran (Millipore Sigma, Burlington, USA) was then spin-coated onto the APTES functionalized surface at 1000 rpm for 20 s. The slides were then heated at 120˚C for 1 hour on a hotplate and then stored until use.

Collagen neutralization

Type I bovine atelocollagen (Nutragen, Advanced Biomatrix, San Diego, USA) (480µl) was diluted to 2.5 mg ml^{-1} in 10X PBS (100µl) (Alfa Aesar, Ward Hill, USA) and ultrapure water (100µl) and then neutralized using 1M NaOH (6µl) (VWR, Randor, USA) to a pH of 7.5. To make a 2.5 mg ml^{-1} collagen solution with 0.5 wt.% of hyaluronic acid (Fisher Scientific, part no AAJ6699303, Pittsburgh, USA), 416 µl of ultrapure water was replaced by a 10mg ml^{-1} hyaluronic acid (HA) solution.

Collagen injection to the microfluidic network

The network was pre-filled with a neutralized (pH = 7.5) 2.5 mg/ml collagen solution using a pipette inserted into port 3 in the large well with all ports open. For the second injection, ports 3 and 5 were closed using adhesive tape and the solution (collagen or collagen/HA blend) was injected at a constant flow rate of 0.5 ml/min from port 2 using a syringe pump. All injections were carried out at 20˚C, before transfer to a 37˚C incubator for gelation.

Rheometry

Rheometry was carried using a hybrid rheometer with a temperature-controlled stage (TA instruments HR-2, Delaware, USA). A 40mm plate geometry was used (TA instruments part no: 113847) with a sample volume of 1.25ml and a gap of 1mm. A fresh neutralized collagen solution was prepared immediately before loading. The temperature was maintained at 21˚C while a 10% strain was applied at 1Hz for 20 minutes. The complex viscosity was measured at 300s, representing the average time between collagen preparation and injection. Representative results are shown in the supplemental information. (Figure S2)

COMSOL simuation

A steady-state 2D simulation was performed using laminar flow physics in COMSOL Multiphysics®. The 2D geometry was designed in Adobe Illustrator (Adobe Systems, California, USA) and imported into COMSOL and a 0.06 mm thickness was applied to the geometry. A fully developed flow rate of 0.5ml/min inlet boundary condition was applied to port 1, while the outlet boundary condition of pressure *(P)* = 0 was applied to ports 2 and 4. No flux boundary conditions were applied to all other boundaries. Free triangular mesh with corner refinements was applied to

the geometry, and a mesh independency study was carried out with stable results at ~541,000 elements. Steady-state velocity magnitude contour was mapped on two lines from ports 1-2 and in the constriction. The strain rate was calculated by determining the slope of the line plot at the required coordinates.

Cell Culture

MDA-MB-231 cells (ATCC, Manassas, USA) were cultured in Dulbecco's modified eagle medium (Gibco, Grand Island, USA) with 10% fetal bovine serum (Gibco, Grand Island, USA) at 37˚C with 95% CO_2. Cells were used between passages 5 and 7. Human adipose-derived stem cells (ADSCs) were cultured in MesenPRO Reduced Serum media supplemented with 1% penicillin and streptomycin. Media was changed every 48 hours. All cell culture reagents and ADSCs were purchased from ThermoFisher Scientific (Waltham, MA, United States). ADSCs were used between passages 3 and 5. Cells were enzymatically dissociated using TrypLE (ThermoFisher Scientific, MA, USA) for 5-7 minutes and centrifuged at 250G for 5 minutes. They were resuspended in 1ml of media. Cells were seeded at a density of 30,000 cm^{-2}.

Immunofluorescence

MDA-MB-231 and ADSCs were fixed after 24 hours of seeding with formaldehyde (3.7%) for 15 mins and stored for 24 hrs in PBS before labeling. Cells were permeabilized in Triton X-100 (0.1%) for 3 min then washed. Cells were treated with Hoechst 33342 (300 nM) (Molecular Probes, USA) for 3 min and 1:400 AlexaFluor 488 conjugated phalloidin (ThermoFisher Scientific, MA, USA) for 15 min to stain nuclei and actin fibers, respectively. Finally, cells were washed and kept under PBS before imaging.

Ultrathin porous parylene membrane fabrication

Ultrathin porous parylene (UPP) membranes were fabricated using our previously published methods[27]. Briefly, six-inch diameter silicon wafers were coated with a water-soluble sacrificial layer of Micro-90 (International Products Corp, NJ, USA), followed by parylene-C deposition using an SCS Labcoter® 2 (Specialty Coating Systems, Indianapolis, IN). Parylene thickness measurement was performed using a Tencore P2 profilometer (KLA-Tencor, Milpitas, CA). Similar to our previous work[28,29] standard photolithography was used to pattern a photoresist layer with hexagonally-packed circular pores with 8 µm diameter and 16 µm center-to-center spacing. This pattern was transferred to the parylene layer using inductively coupled plasma reactive ion etching (ICP-RIE) using a Trion ICP Etcher (Trion Technology, Inc., Tempe, AZ).

Parylene membrane-based channels

Glass slides were sonicated in 70% IPA for 5 minutes and then air-dried. 130 µm thick pressure-sensitive adhesive (PSA) (MP468, 3M Corp, Maplewood, Minnesota, USA) was laser cut to the desired dimensions to define the channel area, then sealed onto the glass slide. A PMMA support frame was attached to the UPP membrane while the UPP was on the silicon wafer. The UPP/PMMA support was then lifted off the wafer by immersion in water to dissolve the sacrificial Micro-90 layer attaching the UPP to the silicon wafer. The UPP/PMMA construct was gently air-dried and then sealed against the top surface of the PSA channel. The finished device consisted of a glass bottom, PSA sidewalls, and a UPP ceiling. The device was sterilized via 15 minutes of UV exposure.

Microscopy and Alignment characterization

Collagen fiber structure was visualized using confocal reflectance microscopy (Leica TCS SP5 II) using a 488nm laser line with a 40x water objective and optical zoom of 1.75x. All settings were constant during the imaging sets. 2µm tall z-stacks were obtained in the center of the 60µm tall channels, each consisting of 13 images. The stacks were processed to an average projection plane before further processing. LOCI CT-FIRE (University of Wisconsin), a MATLAB based curvelet transform package, was used to quantify fiber directionality and anisotropy. Anisotropy was quantified using the coefficient of anisotropy (CoA), which was calculated as the fraction of the fibers lying within $\pm 15^{\circ}$ of the mode compared to the total number of fibers detected. Fiber directionality was reported as an angle relative to the horizontal axis as noted in the text.

Results and Discussion

Flow-induced crystallization (FIC) is an industrial process that takes advantage of conformational changes in response to mechanical strain to enhance the self-assembly of macromolecular subunits (i.e. strain-driven molecular allostery) [17,18]. Recently, Paten et al demonstrated an analogous process to create aligned collagen strands through the controlled extension of a microneedle from a collagen solution. In their elegant experiment, a microneedle was brought into contact with a concentrated neutralized collagen solution and extended away at a controlled rate. The extension of the needle from the surface generated an extensional flow in the necking region of the fluid meniscus between the needle and solution that resulted in the formation of collagen strands with anisotropic fibers [30]. Based on these results, we hypothesized that controlling the strain rate applied to a self-assembling collagen solution within a microfluidic channel network would result in the large-scale alignment of collagen fibers along the flow path.

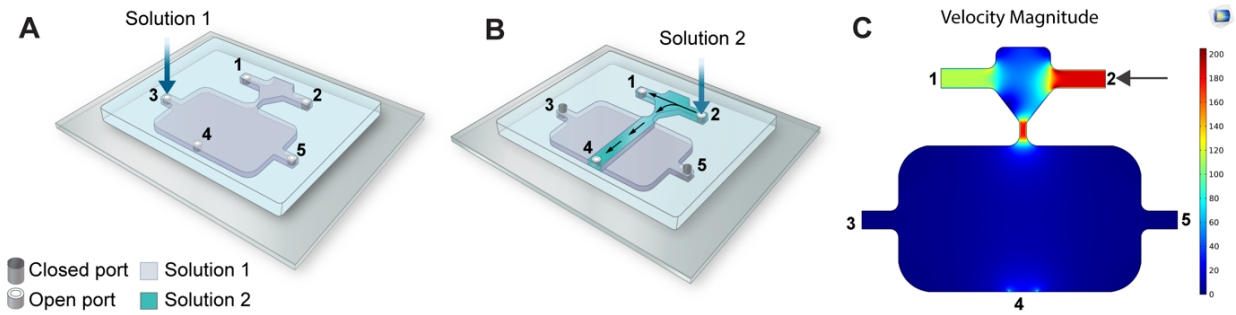

Figure 1: (A) Schematic representation of the microfluidic channel network with port locations is shown. Neutralized collagen I solution is slowly introduced with all ports open until the channel network is filled. (B) Before the collagen solution self-assembles into a gel, the bottom ports (3,5) are closed and the second neutralized collagen solution (solution 2) is injected through port 1 at a defined flow rate. The flow path is shown with arrows. (C) COMSOL simulation showing that the changing channel geometry along the injection path results in local variations of the fluid velocities in the system.

To test our hypothesis, we designed a microfluidic network with varying cross-sectional areas (e.g. constrictions and expansions) and multiple fluid access ports (1 – 5). As shown in **Figure 1A**, the network contained an inlet region (ports 1 – 2), a funnel-shaped constriction with a 10:1 reduction from the top of the funnel to the constriction, and a post-constriction region (ports 3-5). The microfluidic network was first slowly filled with a neutralized collagen type I solution with all ports open at a flow rate of 4µl/min. As shown in **Figure 1B**, the ports in the post-constriction region (3 and 5) were then closed, and a second neutralized collagen solution (or collagen-HA blend) was injected at a defined flow rate following the path 2 - 1 and 2 – 4. The change in the cross-sectional areas of the channel resulted in locally changing fluid velocities (and strain rates) along the flow paths. **Figure 1C** shows the simulated velocity distribution in the inlet region, funnel region, and post-constriction region. From the relation, Q = VA, with a constant solution flow rate *Q,* the average fluid velocity *V* increases at the constriction (decreasing cross-sectional area, A), and V decreases in the post-constriction region (increasing A). Midline velocity profiles in the inlet region and the constriction are shown in **Figure S1.** The COMSOL simulation predicted

a extensional strain rate of 112 s^{-1} from the inlet to the funnel, and a strain rate of 130 s^{-1} at the end of the constriction region.

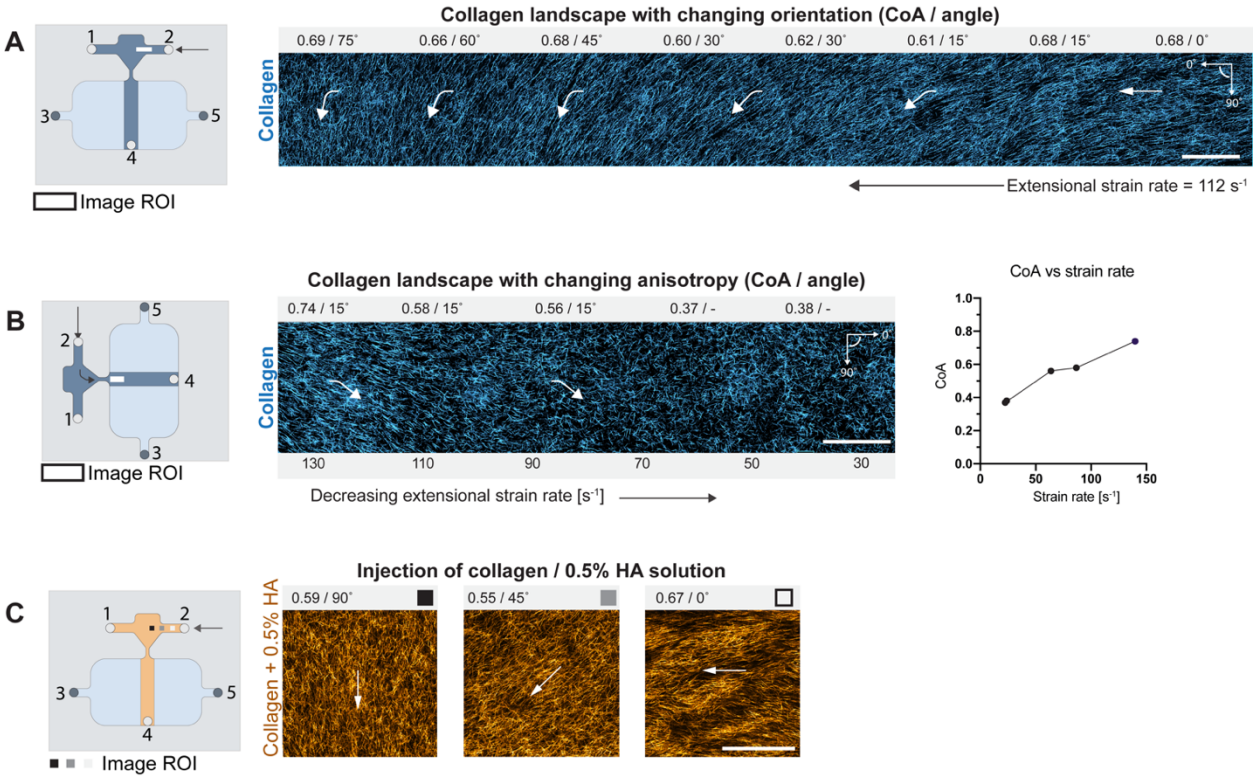

Figure 2: Pseudo colored confocal reflectance images (CRM) showing different collagen landscapes formed within the microfluidic channel after prefilling and injection steps have been carried out. White boxes in schematics are used to mark image ROI, and arrows indicate the direction of fluid flow. (A) The stitched montage of CRM images at the inlet shows that the angle of collagen fiber orientation changes from 0˚ to 75˚ along the flow path (1.5 mm region of interest). Extensional strain rate was calculated to be constant at 112 s^{-1} from the COMSOL simulation velocity profile. (B) The stitched montage of CRM images in the post-constriction region show that a gradient in CoA was produced as a function of the decreasing strain rate. The accompanying plot shows the change of CoA as a function of extensional strain rate. (C) CRM images showing collagen fibers when mixed with 0.5% hyaluronic acid. Colors in header correspond to different regions of interest. Scale bar = 100µm in all images.

The device was then placed in the incubator for 2 hours to promote gel formation before imaging. To quantify collagen fiber properties, confocal reflectance microscopy (CRM) was used to capture 2µm stacks, which were then projected to a single plane. Fiber identification was carried out using LOCI CT-FIRE[31] and the collagen fiber orientation angle and coefficient of anisotropy (CoA) were quantified. **Figure 2A** shows a stitched montage of collagen fibers in the boxed region along the path from 1 – 2. From the COMSOL simulation, the fibers were exposed to a constant strain

rate of 112 s^{-1} along the direction of flow. Subsequent fiber analysis using CT-FIRE over the constituent images of the stitched montage revealed a coefficient of anisotropy (CoA) ranging from 0.69 – 0.60 across the 1.5 mm region of interest (ROI). The fiber orientation angle, reported with respect to the x-axis, shifted from 0˚ to 75˚ as the fluid began to follow path 1-4 toward the constriction. Thus, we were easily able to control the fluid flow path, and control fiber orientation, by opening and closing specific ports in the network. Interestingly, even though the complete collagen injection process lasted on the order of seconds, extensional flows are believed to stretch protein molecules and reduce the activation energy required for self-assembly and enhance fiber nucleation[32]; incubation of the device after injection allowed nucleating fibers to gel in place.

Based on our alignment results, we further hypothesized that if CoA was dependent on the applied extensional strain rate, there should be a threshold strain rate that must be achieved to create alignment. In our system, the injected fluid exiting the constriction and entering the well experienced a dramatic decrease in velocity **(Figure S1).** The change in velocity was found to be non-linear in the constriction exit and therefore, the extensional strain rate decreased rapidly after the post constriction region. **Figure 2B** shows a stitched montage visualizing the decrease in CoA in the direction of fluid flow. A high strain rate of 130 s^{-1} was correlated with a CoA of 0.74, and as the strain rate decreased, the CoA decreased to ~ 0.3. Plotting CoA against strain rate suggested the presence of a threshold strain rate that induced collagen fiber alignment. Our results agree with previous results presented by Paten et al.[30], who inferred that flow-induced crystallization is responsible for the formation of aligned collagen fibrils *in vivo*. The authors also demonstrated that the critical strain rate required to induce fiber alignment would correspond to a minimum Wesseinberg number, $W_e = 1$[33]. The Weissenberg number describes the degree to which

viscoelastic fluids are affected by extensional strain: $W_e=\varepsilon\gamma$, where γ is the material relaxation time, and ε is the strain rate. The relaxation time is defined as the time taken by a polymer chain to release its stored elastic energy. For this experiment, 2.5mg ml^{-1} collagen had a viscosity (v) of approximately 68cP, as determined using rheometry **(Figure S2).** Measurements carried out by Yamakawa et al.[34] showed that relaxation time in dilute collagen solutions scaled linearly with the relation $\gamma= 144(v)$. Therefore, a critical strain rate ε of ~ 100 s^{-1} was calculated to achieve fiber alignment. The strain rates in our fluidic channel were on the order of 100-130s^{-1}, resulting in a maximum $W_e=1.27$ and corresponded to CoA ~ 0.7.

While controlling the structural properties of the ECM is essential in an *in vitro* model, the ECM composition is also unique to the tissue microenvironment. By using a two-stage injection process, we were able to demonstrate the addition of a second ECM material into the microengineered landscape. In **Figure 2C**, the second injection was carried out using a mix of collagen I and 0.5 wt% hyaluronic acid (HA). HA is a common ECM component and is found to be upregulated in the tumor microenvironment. The resulting collagen-HA landscapes exhibited fiber angle and anisotropy similar to pure collagen fibers, and no difference was observed in fiber width or length (figure S3). A slight decrease in the CoA of collagen-HA was observed as compared to pure collagen under the same injection conditions. The two-stage injection technique could also be used to introduce other materials to form multi-material interfaces similar to those found in the native ECM. Thus, using our microfluidic approach, we demonstrated versatile collagen landscape microengineering capabilities, and we turned our attention to address the practical problems associated with integrating cells with gels within a microfluidic system.

Conventional microfluidic systems consist of channels that are permanently bonded to a substrate with fluidic ports being the only point of access to the interior of the system; the introduction of a 3D gel into the channels effectively blocks these initial access ports[35–37]. Cells can be introduced to the system in two common ways: first by pre-mixing them into the ECM solution before injection[37], or second, through the use of peripheral access channels that are separated from the main channel with small constrictions[35]. Including cells in the gel precursor solution limits the extent to which we can further modify fiber properties because changing solution pH, ionic strength, composition, and polymerization temperature can cause cell damage[38–40]. To overcome these limitations, we demonstrate two methods of accessing the microengineered collagen landscape. **Figure 3A** demonstrates a channel functionalization and lift-off technique that allows the microengineered collagen gel to be fully exposed after gelation. The PDMS microfluidic channels were coated with bovine serum albumin to prevent the adhesion of collagen, and the glass substrate was coated with a thin film of poly octadecene alt maleic anhydride (POMA) to promote collagen attachment. After collagen gelation, the channel was lifted off with tweezers to expose

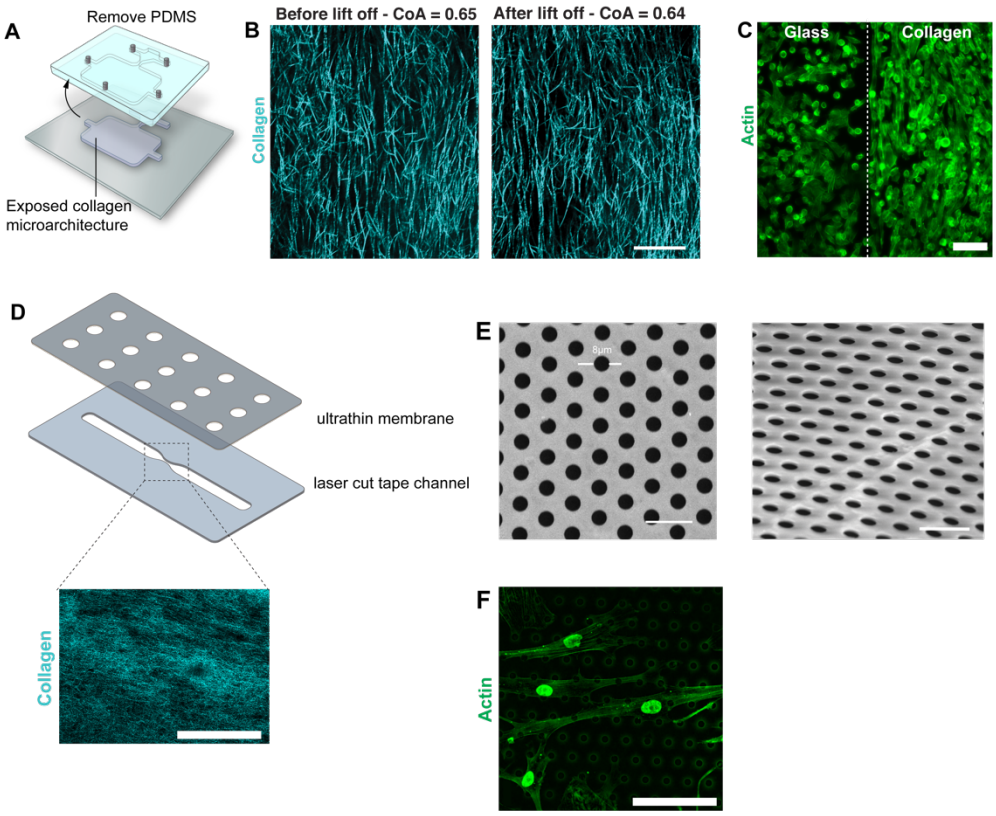

Figure 3: (A) Schematic showing channel lift-off (B) CRM images showing collagen microstructure before and after channel lift-off (scale 25µm) (C) MDA-MB-231 cells cultured on aligned collagen after lift-off and on adjacent glass coverslip (scale 100µm) (D) Device design used to demonstrate the use of an ultrathin membrane with micro-engineered landscape, lower panel shows collagen aligned in the constriction (scale 100µm) (E) SEM micrographs of parylene membrane (scale 50µm) (F) ADSCs cultured on a membrane with underlying collagen (scale 100 µm)

the collagen landscape. The change in CoA of the gel was found to be on the order of 0.01 (**Figure S3**). A representative image of the collagen fibers before and after lift-off can be seen in **Figure 3B**. To demonstrate that cells recognize the collagen fiber structure, MDA-MB-231 cells were patterned onto the exposed collagen landscape. After 24 hours of growth, actin cytoskeleton staining showed that cells oriented themselves parallel to the collagen fibers. The channel lift-off method also adds the potential to introduce secondary channel networks modules on the exposed landscape to provide traditional microfluidic flow and stimulation capabilities[41–43]. While direct access to the engineered collagen landscape is helpful for applications such as studying cell

migration and patterning, advanced culture platforms including organ-on-chip systems are focused on the study of cell-cell and cell-substrate interactions across barrier tissues.

For example, Khire et al investigated leukocyte transmigration across the endothelium and utilized a microfluidic device with a luminal compartment to expose endothelial cells to shear stresses[44,45]. Cells were cultured on a membrane in the luminal side with a collagen gel under the membrane, followed by an abluminal compartment. Similarly, Salminen et al. also reported that the presence of an ECM material under a dual-scale micro/nanoporous membrane increased endothelial cell adhesion on the membrane while the cells were exposed to shear[46]. Co-culture studies in barrier tissues such as the cornea can also benefit from platforms that can allow for cells to be separated from an aligned, engineered ECM using a physical barrier[47]. Therefore, we explored an alternative method for accessing engineered collagen landscapes by using an ultrathin microporous membrane as a "mask" to limit the interaction of cells with the underlying ECM structure. For this application, the PDMS channel was replaced by a combination of laser-cut pressure-sensitive adhesive (sidewalls) and an ultrathin microporous membrane as the "ceiling" as shown in **Figure 3D**. The porous membrane was an 865 nm thick parylene membrane with pore sizes of 8μm and 23% porosity (see SEM image in **Figure 3E**), using techniques described previously[48]. To demonstrate the feasibility of cell growth on the membranes, adipose-derived stem cells (ADSCs) were cultured on the membranes for 24 hours. Cells cultured on membranes atop an aligned collagen gel displayed an elongated morphology which also suggested that substrate sensing could be possible through the large 8μm pores of the membrane. Such a platform could be beneficial for the study of barrier properties in 3D tissue such as in tumor cell intravasation into blood vessels or leukocyte transmigration, and co-culture studies. Using a microporous membrane as a mask,

mechanistic studies to understand the cell-ECM interactions with an aligned landscape are also possible.

Conclusions

In conclusion, we have demonstrated a method to control collagen landscapes using easy to use microfluidic techniques. The use of a channel with different cross-sectional areas showed that the generation of extensional strain aided in collagen fiber alignment and by changing the extensional strain rate, the CoA could be modulated. The direction of collagen fibers was defined by the flow path, which could be controlled by opening or closing specific ports during the injection process. The control over fluid paths can facilitate the formation of multi-material interfaces by exploiting laminar flows and differences in the viscosities of injected solutions. Here, we demonstrated control over structural properties but our approach can be combined with other established collagen tuning techniques such as controlling ionic strength and pH[38,39] and adding molecular crowders to increase the local density of the collagen fibers[49].

Using the channel lift-off process, we demonstrate capabilities to provide direct access to the collagen landscape without the use of complex channel networks. After exposing the collagen landscape, functional channels can also be added on top of the existing collagen landscape to limit cell-substrate interaction, generate chemical gradients, or add new ECM layers for layer-by-layer fabrication of material interfaces, or integrated into an open format, modular microfluidic platform[41,42]. Through the use of an ultrathin membrane "ceiling", we can further study cell-ECM interactions and transmigration across barriers. Using the membrane as a mask to limit the interaction of filopodia with the underlying collagen, future efforts can investigate the prospect of modulating cell-ECM interactions using ultrathin membranes. Our device can, therefore, provide

a versatile platform with control over collagen landscapes and enable easy access to the 3D collagen gel for biomimetic tissue studies in-vitro. We expect our platform to be of benefit to researchers in the field of tissue engineering, biomaterials, and cell physiology due to its adaptability and ease of use.

Acknowledgements

The authors acknowledge support from the Kate Gleason College of Engineering New Faculty Startup Funds to V.V.A, NIH project R35GM119623 to T.R.G., and NIH project R01DC014568 to D.A.B. The authors acknowledge Dr. Hyla Sweet from the Confocal Microscopy Lab, and Dr. Christopher Lewis and Mr. Tom D. Allston from the Materials Characterization Laboratory. We also acknowledge Zahra Allahyar for cell culture assistance and thank Fei Rost for illustration support.

References:

[1] C. Frantz, K. M. Stewart, V. M. Weaver, *J Cell Sci* **2010**, *123*, 4195.
[2] T. R. Cox, J. T. Erler, *Dis Model Mech* **2011**, *4*, 165.
[3] P. Lu, K. Takai, V. M. Weaver, Z. Werb, *Csh Perspect Biol* **2011**, *3*, a005058.
[4] H. C. Pruitt, D. Lewis, M. Ciccaglione, S. Connor, Q. Smith, J. W. Hickey, J. P. Schneck, S. Gerecht, *Matrix Biol* **2019**, DOI 10.1016/j.matbio.2019.02.003.
[5] E. S. Lai, N. F. Huang, J. P. Cooke, G. G. Fuller, *Regen Med* **2012**, *7*, 649.
[6] A. Islam, M. Younesi, T. Mbimba, O. Akkus, *Adv Healthc Mater* **2016**, *5*, 2237.
[7] B. R. Seo, X. Chen, L. Ling, Y. H. Song, A. A. Shimpi, S. Choi, J. Gonzalez, J. Sapudom, K. Wang, R. C. A. Eguiluz, D. Gourdon, V. B. Shenoy, C. Fischbach, *Proc National Acad Sci* **2020**, 201919394.
[8] E. Brauer, E. Lippens, O. Klein, G. Nebrich, S. Schreivogel, G. Korus, G. N. Duda, A. Petersen, *Adv Sci* **2019**, *6*, 1801780.
[9] M. W. Conklin, J. C. Eickhoff, K. M. Riching, C. A. Pehlke, K. W. Eliceiri, P. P. Provenzano, A. Friedl, P. J. Keely, *Am J Pathology* **2011**, *178*, 1221.
[10] P. P. Provenzano, D. R. Inman, K. W. Eliceiri, J. G. Knittel, L. Yan, C. T. Rueden, J. G. White, P. J. Keely, *Bmc Med* **2008**, *6*, 11.
[11] C. Guo, L. J. Kaufman, *Biomaterials* **2007**, *28*, 1105.
[12] S. P. Carey, A. Starchenko, A. L. McGregor, C. A. Reinhart-King, *Clin Exp Metastasis* **2013**, *30*, 615.
[13] T. S. Girton, V. H. Barocas, R. T. Tranquillo, *J Biomechanical Eng* **2002**, *124*, 568.
[14] J. A. M. Nuhn, A. M. Perez, I. C. Schneider, *Acta Biomater* **2018**, *66*, 248.
[15] A. Ray, Z. M. Slama, R. K. Morford, S. A. Madden, P. P. Provenzano, *Biophys J* **2017**, *112*, 1023.
[16] A. Ray, R. K. Morford, N. Ghaderi, D. J. Odde, Paolo. P. Provenzano, *Integr Biol* **2018**, *10*, 100.
[17] J. A. Matthews, G. E. Wnek, D. G. Simpson, G. L. Bowlin, *Biomacromolecules* **2002**, *3*, 232.
[18] Y. Wakuda, S. Nishimoto, S. Suye, S. Fujita, *Sci Rep-uk* **2018**, *8*, 6248.
[19] B. A. Nerger, P.-T. Brun, C. M. Nelson, *Soft Matter* **2019**, *15*, 5728.
[20] S. Rhee, J. L. Puetzer, B. N. Mason, C. A. Reinhart-King, L. J. Bonassar, *Acs Biomater Sci Eng* **2016**, *2*, 1800.
[21] A. Anielski, E. K. B. Pfannes, C. Beta, *Review Of Scientific Instruments* **2017**, *88*, DOI 10.1063/1.4978535.
[22] I. Meyvantsson, D. J. Beebe, *Annu Rev Anal Chem* **2008**, *1*, 423.
[23] P. Lee, R. Lin, J. Moon, L. P. Lee, *Biomed Microdevices* **2006**, *8*, 35.
[24] N. Saeidi, E. A. Sander, J. W. Ruberti, *Biomaterials* **2009**, *30*, 6581.
[25] C. Haynl, E. Hofmann, K. Pawar, S. Förster, T. Scheibel, *Nano Lett* **2016**, *16*, 5917.
[26] T. Pompe, L. Renner, M. Grimmer, N. Herold, C. Werner, *Macromol Biosci* **2005**, *5*, 890.
[27] S. Gholizadeh, Z. Allahyari, R. Carter, L. Delgadillo, M. Blaquiere, F. Nouguier-Morin, N. Marchi, T. R. Gaborski, *bioRxiv* **2020**.
[28] Z. Allahyari, S. Gholizadeh, H. H. Chung, L. F. Delgadillo, T. R. Gaborski, *Acs Biomater Sci Eng* **2019**, *6*, 959.

[29] A. R. Mazzocchi, A. J. Man, J.-P. S. DesOrmeaux, T. R. Gaborski, *Cel. Mol. Bioeng.* **2014**, *7*, 369.
[30] J. A. Paten, S. M. Siadat, M. E. Susilo, E. N. Ismail, J. L. Stoner, J. P. Rothstein, J. W. Ruberti, *Acs Nano* **2016**, *10*, 5027.
[31] J. S. Bredfeldt, Y. Liu, C. A. Pehlke, M. W. Conklin, J. M. Szulczewski, D. R. Inman, P. J. Keely, R. D. Nowak, T. R. Mackie, K. W. Eliceiri, *J Biomed Opt* **2014**, *19*, 016007.
[32] C. Seifert, F. Gräter, *Biochimica Et Biophysica Acta Bba - Gen Subj* **2013**, *1830*, 4762.
[33] F. H. M. Nestler, S. Hvidt, J. D. Ferry, A. Veis, *Biopolymers* **1983**, *22*, 1747.
[34] H. Yamakawa, *Macromolecules* **1975**, *8*, 339.
[35] Alex, ra Boussommier, R. D. Kamm, *Cancer Immunology Research* **2016**, *4*, B165.
[36] S. Bersini, J. S. Jeon, G. Dubini, C. Arrigoni, S. Chung, J. L. Charest, M. Moretti, R. D. Kamm, *Biomaterials* **2014**, *35*, 2454.
[37] W. Han, S. Chen, W. Yuan, Q. Fan, J. Tian, X. Wang, L. Chen, X. Zhang, W. Wei, R. Liu, J. Qu, Y. Jiao, R. H. Austin, L. Liu, *Proc National Acad Sci* **2016**, *113*, 11208.
[38] K. E. Sung, G. Su, C. Pehlke, S. M. Trier, K. W. Eliceiri, P. J. Keely, A. Friedl, D. J. Beebe, *Biomaterials* **2009**, *30*, 4833.
[39] J. R. Harris, A. Soliakov, R. J. Lewis, *Micron* **2013**, *49*, 60.
[40] A. J. Holder, N. Badiei, K. Hawkins, C. Wright, P. R. Williams, D. J. Curtis, *Soft Matter* **2018**, *14*, 574.
[41] J. Yu, E. Berthier, A. Craig, T. E. de Groot, S. Sparks, P. N. Ingram, D. F. Jarrard, W. Huang, D. J. Beebe, A. B. Theberge, *Nat Biomed Eng* **2019**, *3*, 830.
[42] V. V. Abhyankar, M. Wu, C.-Y. Koh, A. V. Hatch, *Plos One* **2016**, *11*, e0156341.
[43] U. N. Lee, J. H. Day, A. J. Haack, R. C. Bretherton, W. Lu, C. A. DeForest, A. B. Theberge, E. Berthier, *Lab Chip* **2020**, *20*, 525.
[44] T. S. Khire, A. T. Salminen, H. Swamy, K. S. Lucas, M. C. McCloskey, R. E. Ajalik, H. H. Chung, T. R. Gaborski, R. E. Waugh, A. J. Glading, J. L. McGrath, *Cell Mol Bioeng* **2020**, *13*, 125.
[45] H. H. Chung, C. K. Chan, T. S. Khire, G. A. Marsh, A. Clark, R. E. Waugh, J. L. McGrath, *Lab Chip* **2014**, *14*, 2456.
[46] A. T. Salminen, J. Zhang, G. R. Madejski, T. S. Khire, R. E. Waugh, J. L. McGrath, T. R. Gaborski, *Small Weinheim Der Bergstrasse Ger* **2019**, *15*, e1804111.
[47] M. Hirsch, G. Prenant, G. Renard, *Exp Eye Res* **2001**, *72*, 123.
[48] S. Gholizadeh, Z. Allahyari, R. Carter, L. Delgadillo, M. Blaquiere, F. Nouguier-Morin, N. Marchi, T. R. Gaborski, *Biorxiv* **2020**, 2020.05.07.083188.
[49] V. Magno, J. Friedrichs, H. M. Weber, M. C. Prewitz, M. V. Tsurkan, C. Werner, *Acta Biomater* **2017**, *55*, 109.